ISSN 2281-4299

DIPARTIMENTO DI INGEGNERIA INFORMATICA
AUTOMATICA E GESTIONALE ANTONIO RUBERTI

SAPIENZA
UNIVERSITÀ DI ROMA

PDE based inpainting algorithms: performance evaluation of the Cahn-Hillard model

Alberto De Santis
Roberto Castorrini

Technical Report n. 3, 2016

PDE based inpainting algorithms: performance evaluation of the Cahn-Hillard model

Alberto De Santis*and Roberto Castorrini†

August 30, 2016

Abstract

Image inpainting consists in restoring a missing or a damaged part of an image on the basis of the signal information in the pixels surrounding the missing domain. To this aim a suitable image model is needed to represent the signal features to be reproduced within the inpainting domain, also depending on the size of the missing area. With no claim of completeness, in this paper the main streamline of the development of the PDE based models is retraced. Then, the Cahn-Hillard model for binary images is analyzed in detail and its performances are evaluated on some numerical experiments.

Keywords: Image inpainting, image processing, functional convexity splitting, unconditionally stable numerical scheme.

*Department of Computer, Control, and Management Engineering - Sapienza University of Rome, Via Ariosto 25, 00185 Roma, Italy, desantis@dis.uniroma1.it.

†Sapienza University of Rome, castorrini.1278671@studenti.uniroma1.it

1 Introduction

Inpainting process has been known for a long time: a missing/damaged area within an image is reconstructed in order to recover its visual quality. Originally dedicated to the restoration of artistic works (retouching), it has nowadays spread in many areas due to the success of digital imaging: restoring photos from scratches or text overlays, recovery from loss due to impaired image transmission, object disocclusion of pictures, removing logos from videos, just to mention a few. Since the image signal within the occluded area is completely unknown, the problem of inpainting can be solved only by assuming suitable priors on the image features that are likely shared between the occluded and non-occluded parts. Generally speaking an image can be modeled as the collection of homogeneous structures (shapes, objects, texture) separated by sharp edges. Image priors therefore have either local nature, like the geometrical structures, or global nature like the textures. These features need to be smoothly continued inside the occluded or missing domain. As pointed out in [1], two main approaches to the image inpainting problem has been developed, according to the nature of the information to be propagated: the variational image inpainting and the texture synthesis. Variational image inpainting is focused on the continuity of the geometrical structures of an image that are evolved by means of partial differential equations (PDE) models; these methods generally have good performances in filling narrow gaps in piecewise smooth images, see for instance [2]. Texture synthesis deals with the problem of producing new instances of a texture from a smaller sample, and therefore can be applied to the inpainting of images characterized by many textured (non-smooth) areas, [3]. As real images contain both smooth and texture properties, combined methods in image inpainting were also developed to exploit features from both main approaches in different ways and go by the name of image completion [4], [5].

This work lies within the variational inpainting framework, and a survey of the most influential papers will be given. It is acknowledged that Bertalmio et. al. [6] pioneered the inpainting problem in digital image processing. The authors model the professional restorators inpaint artwork that follows some basic principles

- Inpainting is supposed to restor the original picture visual quality and unity.
- The structure of the area surrounding the missing domain is continued into the gap, contour lines are drawn via the prolongation of those

arriving at the boundary.

- Every structure part inside the region is filled with colour that matches its colours at the missing domain boundary.
- Texture is added to the inpainted area.

Referring to gray scale images for simplicity, let Ω be the domain to be inpainted, and $\partial\Omega$ its boundary; the idea is to propagate the constant gray level lines (isophotes) from outside Ω to inside in an iterative manner producing a sequence $I^n(i,j)$ of improved images that converge as n increases to a restored version of the initial damaged image $I^0(i,j)$

$$I^{n+1}(i,j) = I^n(i,j) + \Delta t I_t^n(i,j), \quad \forall (i,j) \in \Omega$$

where (i,j) denote the image pixel, n is the *inpainting time*, Δt is the rate of improvement, $I_t^n(i,j)$ is the update of $I^n(i,j)$. This term is constructed by an image smoothness estimator given by the discrete Laplacian $L_n(i,j) = I_{xx}^n(i,j) + I_{yy}^n(i,j)$ whose variation $\delta L_n(i,j)$ is propagated along the direction given by the discretized image gradient $\nabla I^n(i,j)$ which is orthogonal to the isphotes direction given by $\nabla^\perp I^n(i,j)$

$$I_t^n(i,j) = (\delta L_n(i,j) \cdot \frac{\nabla^\perp I^n(i,j)}{|\nabla^\perp I^n(i,j)|} |\nabla I^n(i,j)|$$

Since the direction field $\nabla^\perp I^n(i,j)/|\nabla^\perp I^n(i,j)|$ is not a priori known but is progressively estimated, to prevent isphotes to cross each other, every few steps of the inpainting algoritm an anisotropic diffusion is applied ([7]) to also maintain the image sharpness

$$\frac{\partial I}{\partial t}(x,y,t) = g_\epsilon(x,y) k(x,y,t) |\nabla I(x,y,t)|, \quad \forall x,y \in \Omega^\epsilon$$

where $k(x,y,t)$ is the euclidean curvature of the isophotes, Ω^ϵ is the dilation of Ω with a ball of radius ϵ, and g_ϵ is a smooth function with value 0 on $\partial\Omega^\epsilon$ and with value 1 in Ω (to impose Dirichlet boundary conditions).

Figure 1 shows the general result obtainable on a color image (the algorithm is applied on any color plane independently) showing a good visual result, on the detail of Figure 2 some drawback is highlighted.

Similar concepts can be found in [2] and [8]. In the former the inpainting problem is formulated as a disocclusion problem. The authors define the T-junctions, the points where visible edges intersect the occluding objects. Pairs of T-junctions must be connected, which belong to the same edge

Figure 1: Example of inpainting of a color image with no large gaps by the Bertalmio et al. algorithm; the picture is taken from [6].

Figure 2: A detail of the previous picture showing a blurring effect with an insufficient diffusion; the picture is taken from [1].

hidden behind the occluding object. As pointed out in [1], curvature is not preserved at the boundary of the occluding domain, and a simple topology (no holes allowed) is required, therefore the method is only applicable to narrow gaps. In the latter paper the dynamical model introduced in [6] is shown to have a strong connection with two dimensional fluid dynamics based on the Navier-Stokes equations. Indeed it is equivalent to the inviscid Euler equations for incompressible flow.

A different approach was proposed in [9] where a Total Variation (TV) method is presented, stemming from the classical restoration model of Rudin et. al. [10]. This method searches for a function $\hat{I}(x, y)$ of bounded variation on Ω that minimize the functional of the total variation on the image domain D (first term in the integral) with a constraint given by a fidelity term (second term in the integral)

$$TV(\hat{I}) = \int_D |\nabla \hat{I}(x, y)| dxdy + \lambda \int_{D \setminus \Omega} (I(x, y) - \hat{I}(x, y))^2 dxdy$$

This model can propagate sharp edges within the missing domain but,

because of the regularization term (first term in the integral), the length of the edges is penalized and therefore can not propagate through large areas; moreover there are some connectivity problems since the direction of isophotes is not extended with continuity across $\partial\Omega$. The authors amended these drawbacks in [11], where a new regularization term is adopted that penalizes the integral of the square of the curvature along the isophotes (Euler's elastica). Let $\hat{I}$ be an admissible inpainting of image I, along any isophote curve $\gamma_\lambda : \hat{I} = \lambda$ the curvature is defined as

$$k = \nabla \cdot \overrightarrow{n} = \nabla \cdot \frac{\nabla \hat{I}}{|\nabla \hat{I}|}$$

Along the length element dt in the normal direction $\overrightarrow{n}$ we have that

$$d\lambda = |\nabla \hat{I}| dt$$

and therefore the integrated elastica energy extended on $\hat{I}$ is

$$\int_0^1 w(\lambda) \int_{\gamma_\lambda : \hat{I} = \lambda} (a + bk^2) ds d\lambda = \int_D w(\hat{I}) \left(a + b\big(\nabla \cdot \frac{\nabla \hat{I}}{|\nabla \hat{I}|}\big)^2 \right) |\nabla \hat{I}| dx dy$$

where a, b are two positive constant weights. For piece-wise smooth images (non texture images) function w should weigh more the edges, therefore it should assume the value zeros within the homogeneous objects of the scene, and the value one on the edges. A possible choice could be $w(\lambda) = (1 - h(\lambda))$, where $h(\lambda)$ is the image histogram. The new ealstica formulation guarantees that the isophotes can be connected across large areas and their direction is kept continuous across $\partial\Omega$. Numerical experiments on phantom images show the difference betweem TV and Elastica inpainting (see Figure 3).

Following the argument developed in [11], Esedoglu and Shen ([12]) adapt to the inpainting problem the Munford-Shah model for image segmentation [13]. By adopting the elliptic approximation to the Mumford-Shah model developed in [14], they obtain equations where the highest order derivatives are linear and therefore deliver a fast numerical scheme that, anyway, penalizes the length of edges, preventing its application to large gaps. Therefore the Euler elastica correction is adopted as in [11] that penalizes the square of the curvature along the edges.

Bertozzi et al. [16], propose a model that features some of the interesting properties of model developed in [12], but less involved and delivering a fast numerical scheme for the solution. This model is analyzed in detail in the next Section and its performances will be tested in some numerical experiments. Some conclusions and possible developments will be discussed.

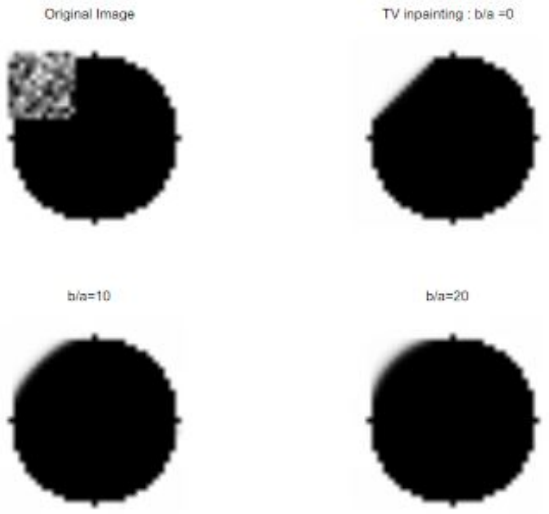

Figure 3: A large weight b against the curvature term delivers a better visual quality in term of smoothness of egdes and isophotes; the picture is taken from [11].

2 The Cahn-Hillard model

In order to approch fourth-order inpainting algorithms, in [16] is proposed a modified Cahn-Hilliard model for the evolution of the inpainted version I of the damaged image $I^0 \in L^2(D)$:

$$\begin{cases} \frac{\partial I}{\partial t} = -\Delta(\varepsilon \Delta I - \frac{1}{\varepsilon} W'(I)) + \lambda(x)(I^0 - I), \qquad (t,x) \in \mathbb{R} \times D \\ \lambda(x) = \chi_{D \setminus \Omega}(x) \lambda_0 \\ W(u) = u^2(1-u)^2. \end{cases} \tag{1}$$

where χ_A represent the indicator function of the set A (we recall from the previous section that Ω is the domain to be inpainted). Here W is a potential with wells corresponding to different grayscale values. In our case W has wells at values 0 and 1, so we describe the simplest model concerning binary images. The difference between the standard Cahn-Hilliard model (which describes the process of phase separation of a binary fluid) and model (1) is the so called *fidelity term* $\lambda(x)(I^0 - I)$. Its role is to keep the solution

of the model close to the initial data I^0 in $D \setminus \Omega$, where a complete image information is available.

In [17] has been proved the existence of a unique global weak solution of (1) belonging to $\mathcal{C}([0,T]; L^2(D) \cap L^2([0,T], H_0^2))$ where

$$H_0^2(D) := \{u \in H^2(D) \quad | \quad \frac{\partial u}{\partial \nu} = 0 \quad \text{on} \quad \partial D\}.$$

Further the authors showed that in the limit $\lambda_0 \to \infty$, for any given initial data $I^0 \in C^2(D)$, a stationary solution of (1) solves the problem

$$\begin{cases} -\Delta(\varepsilon \Delta I - \frac{1}{\varepsilon} W'(I)) = 0, & \text{on} \quad \Omega \\ \\ I = I^0 & \text{on} \quad \partial\Omega \\ \\ \nabla I = \nabla I^0 & \text{on} \quad \partial\Omega \end{cases} \tag{2}$$

which points out a fundamental property of inpainting models described in the previous section, such as the smooth continuation of the isophotes into the missing domain.

Despite the advantages of not dealing with curvature based model, the main difficulty, because of the fidelity term, is that equation (1) is not a gradient flow in some Banach space. A possible strategy is to consider the *convexity splitting* idea [18]. In fact we know that the standard Cahn-Hilliard equation is a gradient flow in H^{-1} for the functional

$$\mathcal{L}_1(I) = \int_\Omega \frac{\varepsilon}{2} |\nabla I|^2 + \frac{1}{\varepsilon} W(I) dx. \tag{3}$$

On the other hand it is easy to verify that $\lambda(I^0 - I)$ is a gradient flow in L^2 for the energy:

$$\mathcal{L}_2(I) = \frac{1}{2} \int_\Omega \lambda(x)(I^0 - I)^2 dx, \tag{4}$$

so we can think to split both $\mathcal{L}_1$ and $\mathcal{L}_2$ into convex functionals. A possible choice proposed in [16] is, for example

$$\mathcal{L}_1 = \mathcal{L}_{1,a} - \mathcal{L}_{1,b} = \int_\Omega \frac{\varepsilon}{2} |\nabla I|^2 + \frac{C_1}{2} |I|^2 dx - \int_\Omega -W(I) + \frac{C_2}{2} |I|^2 dx \tag{5}$$

$$\mathcal{L}_2 = \mathcal{L}_{2,a} - \mathcal{L}_{2,b} = \int_D \frac{C_2}{2} |I|^2 dx - \frac{1}{2} \int_D -\lambda(x)(I^0 - I)^2 + \frac{C_2}{2} |I|^2 dx \tag{6}$$

In order to guarantee the convexity of these functionals, $\mathcal{L}_{i,j}$ must satisfy the following inequality for all $i = 1, 2$ and $j = a, b$:

$$\langle D^2(\nabla \mathcal{L}_{i,j})(I)I, I\rangle_{\mathcal{B}} > l > 0 \tag{7}$$

where D^2 represents the second variation and $\langle \cdot, \cdot \rangle_{\mathcal{B}}$ is the inner product defined in the Banach space $\mathcal{B}$ (we work with L^2 or H^{-1} depending on the energy). The convexity condition (7) is ensured by choosing the positive constants such that

$$C_1 > \frac{1}{\varepsilon} \quad \text{and} \quad C_2 > \lambda_0.$$

The splitting (3) and (4) leads to the following discrete time-stepping scheme

$$\frac{I^{n+1} - I^n}{\Delta t} = -\nabla_{H^{-1}} \left(\mathcal{L}_{1,a}(I^{n+1}) - \mathcal{L}_{1,b}(I^n)\right) - \nabla_{L^2} \left(\mathcal{L}_{2,a}(I^{n+1}) - \mathcal{L}_{2,b}(I^n)\right),$$

corresponding to the numerical scheme

$$\begin{aligned} \frac{I^{n+1}(x) - I^n(x)}{\Delta t} &+ \varepsilon \Delta \circ \Delta I^{n+1}(x) - C_1 \Delta I^{n+1}(x) + C_2 I^{n+1}(x) \\ &= \Delta \left(\frac{1}{\varepsilon} W'(I^n(x)) \right) + \lambda(x)(I^0(x) - I^n(x)) \\ &- C_1 \Delta I^n(x) + C_2 I^n(x). \end{aligned} \tag{8}$$

By the results of their numerical tests, the authors in [16] inferred the unconditional stability of the scheme (8). It is worth noting that, as pointed out before, this model is not given by a gradient flow, so the definition of stability is not the standard one ([15]). Precisely a numerical scheme corresponding to those kind of evolution equation is unconditionally stable if, for any time step Δt, there exist $0 < T < \infty$ such that for all $k\Delta t \leq T$ the solutions of (8) are bounded in $[0, T]$.

In order to compute I^{n+1} we want to use the cosine discrete transform (see [19]) assuming Neumann boundary condition

$$\frac{\partial I^{n+1}}{\partial \nu}(x) = \frac{\partial \Delta I^{n+1}}{\partial \nu}(x) = 0, \qquad \forall x \in \partial\Omega. \tag{9}$$

The transform coefficients of I^n are

$$\hat{I}^n_{i,j} = \alpha_i \beta_j \sum_{r=1}^{M} \sum_{s=1}^{N} I^n_{r,s} \cos \frac{(2r-1)(i-1)\pi}{2M} \cos \frac{(2s-1)(j-1)\pi}{2N} \tag{10}$$

for given data $\{I^n_{r,s} | r = 1, \cdots, M; s = 1, \cdots N\}$. In the previous equation α_i and β_j are given by

$$\alpha_i = \begin{cases} \sqrt{\frac{1}{M}}, & i = 1 \\ \sqrt{\frac{2}{M}}, & i \in [2, M] \end{cases} \quad \text{and} \quad \beta_j = \begin{cases} \sqrt{\frac{1}{N}}, & j = 1 \\ \sqrt{\frac{2}{N}}, & j \in [2, N]. \end{cases} \tag{11}$$

Taking $(x, y) \in [0, l_x] \times [0, l_y]$, in the discrete cosine space the Laplacian reads

$$\Delta I(x, y, k\Delta t) = -\sum_{i=1}^{M} \sum_{j=1}^{N} \left(\lambda_i^2 + \lambda_j^2\right) \alpha_i \beta_j \hat{I}^n_{i,j} \cos(\lambda_i x) \cos(\lambda_j y)$$

where

$$\lambda_i = \frac{(i-1)\pi}{l_x} \quad \text{e} \quad \lambda_j = \frac{(j-1)\pi}{l_y}.$$

Putting the last results in the numerical scheme (8) we obtain an explicit equation for the coefficients $\hat{I}^{n+1}_{i,j}$:

$$\hat{I}^{n+1}_{i,j} = \frac{(1 - C_1 \Delta t A_{ij} + C_2 \Delta t)\hat{I}^n_{i,j} + \frac{\Delta t}{\varepsilon} \Delta \widehat{W}'(I^n_{i,j}) + \Delta t \lambda (I^0 - \hat{I}^n_{i,j})}{1 + C_2 \Delta t + \varepsilon \Delta t A^2_{ij} - C_1 \Delta t A_{ij}}$$

with $A_{ij} = \lambda_i^2 + \lambda_j^2$. Finally, from (10), we recover $I^{n+1}_{r,s}$ by means of the inverse of the discrete cosine transform:

$$I^{n+1}_{r,s} = \sum_{i=1}^{M} \sum_{j=1}^{N} \alpha_r \beta_s \hat{I}^{n+1}_{i,j} \cos \frac{\lambda_r (2i-1) l_x}{2M} \cos \frac{\lambda_s (2j-1) l_y}{2N}.$$

3 Numerical experiments

In this section numerical results are presented. We implemented the numerical scheme (8) in a MATLAB code. The corresponding numerical scheme obtained by assuming Dirichlet boundary conditions is implemented too, presenting results on the same examples. As test binary image we chose a black square of size $N = 300$, with a white circle of radius $r = 80$ in the centre. Starting from this picture, some inpainting domains (the gray zone) have been builted, using squares and strips, which are easier to treat with binary inpainting Cahn-Hilliard model. For each example we report three different pictures representing the initial data, the intermediate state after

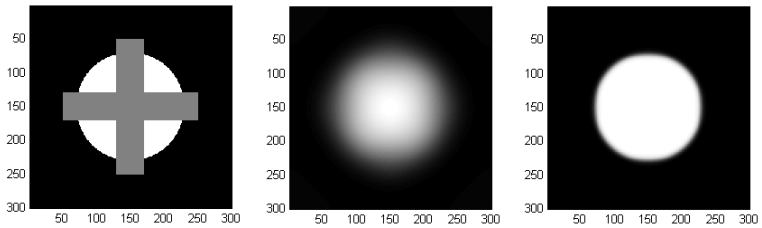

Figure 4: Cross, Neumann boundary conditions. Parameters: $\lambda_0 = 10^5$; $\varepsilon = 0.8$; $\varepsilon' = 0.01$; $C_1 = 300$; $C_2 = 3 \cdot \lambda_0$.

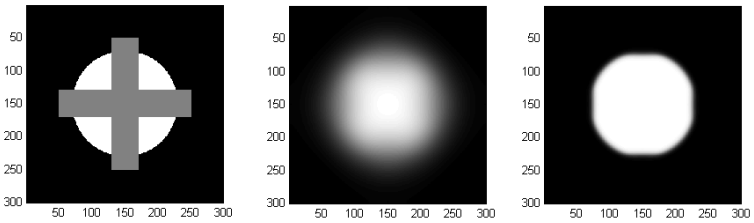

Figure 5: Cross, Dirichlet boundary conditions. Parameters: $\lambda_0 = 10^5$; $\varepsilon = 0.8$; $\varepsilon' = 0.01$; $C_1 = 300$; $C_2 = 3 \cdot \lambda_0$.

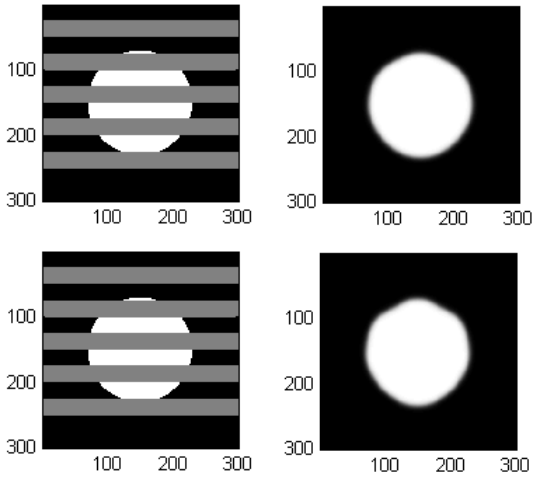

Figure 6: Strips, Neumann conditions (first row), Dirichlet condition (second row).

$n = 100$ steps with ε fixed and a finally state achived after 100 steps more, with ε updated to a smaller value ε'.

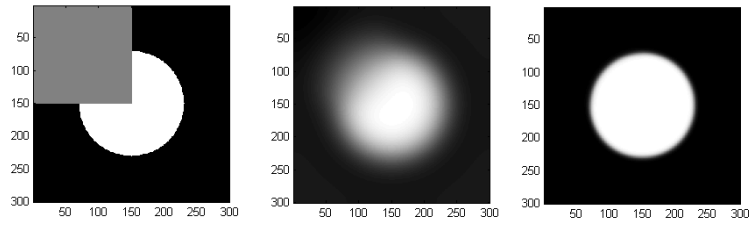

Figure 7: Square, Neumann boundary conditions.

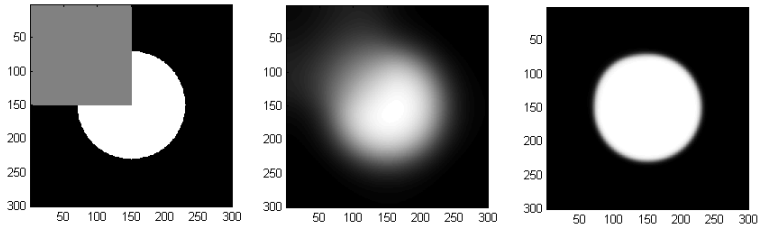

Figure 8: Square, Dirichlet boundary conditions.

Figures 4-5 show the results for an inpainted region given by a cross in the centre of the test image, assuming Neumann and Dirichlet condition rispectively, and assuming initial condition zero on the inpainting region. We can see in this case that the algorithm with Neumann condition performs better than the one with Dirichlet conditions because of the smooth continuation of the derivative on the border. We can value this difference much better with an inpainting region given by several strips (Figure 6). Neverthless we can improve the result a little bit choosing $\lambda_0 = 10^4$. Finally in Figures 7-8 is reported one of the example presented in [16], in which the authors used a Fast Fourier Transform (fft2 in MATLAB) method. The parameters are setting as before, and the result with Dirichlet boundary condition is good as the Neumann one, due to the uniformity of the inpainting region.

As a further experiment we simply increased the number of iterations to achieve a better reconstruction accuracy. In Figure 9 the same experiment of Figure 4 is reported with $n = 200$ iterations, and in Figure 10 the experiment of Figure 5 is reported with $n = 400$ iterations. In both cases we can appreciate a substantial improvement of the reconstruction, again with a better performance in the Neumann case as compared to the Dirichlet one.

As a general remark we can say that, while the inpainting algorithm has a satisfactory behavior in many different situations, indeed the same parameters setting provides better performances on some test as compared

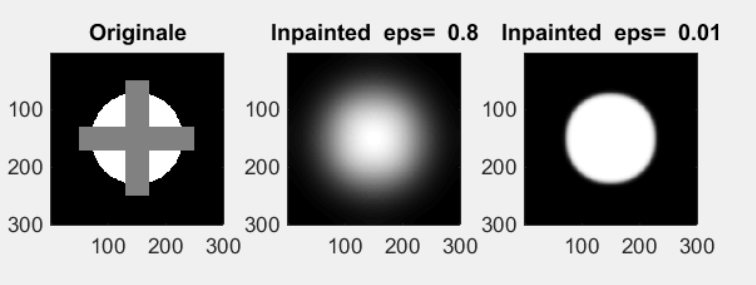

Figure 9: Cross, Neumann boundary conditions. Parameters: $\lambda_0 = 10^5$; $\varepsilon = 0.8$; $\varepsilon' = 0.01$; $C_1 = 300$; $C_2 = 3 \cdot \lambda_0$.

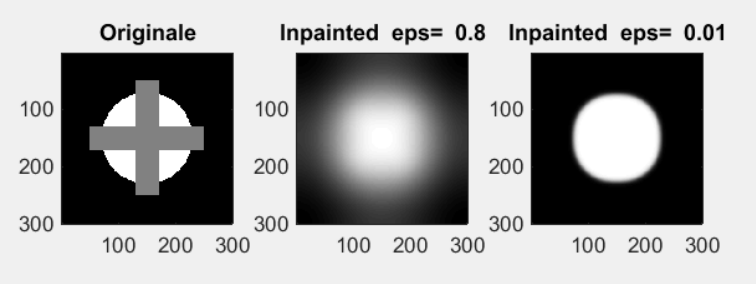

Figure 10: Cross, Dirichlet boundary conditions. Parameters: $\lambda_0 = 10^5$; $\varepsilon = 0.8$; $\varepsilon' = 0.01$; $C_1 = 300$; $C_2 = 3 \cdot \lambda_0$.

to others. For instance, tests of Figures 7-8 denote a better boundary reconstruction than in the other cases. Moreover there are even some fine differences between Figure 7 and 8, at a closer visual inspection the former seems to better reconstruct the white disk. Therefore, while the numerical scheme is unconditionally stable and therefore as n increases a bounded solution is obtained, the accuracy of the inpainting area reconstruction depends on the parameters setting, that therefore need to be tuned for any particular experiment.

4 Conclusion

In this work a sufficiently complete survey on image inpainting methods in provided, by highlighting the points of strength and weakness of each of them. Within the framework of the variational methods we focused on the Cahn-Hilliard model that, avoiding the involved mathematics typical of vari-

ational models, maintains the ability to deliver a good inpainting comparable to the more complex models, but in a simpler and faster way. The rapidity mainly depends on the splitting of the energy functional to be minimized in a convex term and a concave one. This convexity splitting procedure delivers a fast numerical scheme for the computation of the optimal solution, based on FFT, that is unconditionally stable. Indeed, we used the cosine transform instead of the FFT and obtained a fast numerical scheme as well. In all the numerical experiments formed with different inpainting domains a general setting for the algorithm was found that gave satisfactory results both in terms of convergence rate and accuracy of the reconstruction. Nevertheless a given setting may well feature better performances in some tests than in others, suggesting that the parameters setting is an issue to improve the accuracy of the optimal solution. As a final remark, the algorithm is designed to deal with high contrast binary images but in a further investigation it can be well extended to images with more that two levels. To this aim two possible techniques can be adopted: a nonlinear potential function W can be designed with wells in any of the image level and applying the same algorithm; a multilevel image is usually obtained by a segmentation of an original picture by applying successive binarization, and therefore to each stage the Cahn-Hilliard model can be applied with the binary potential.

References

[1] I. B. Fidaner, A Survey on Variational Image Inpainting,Texture Synthesis and Image Completion, *https://fidaner.files.wordpress.com/2013/10/survey_draft3.pdf*, (2013).

[2] S. Masnou,J. M. Morel, Level lines based disocclusion, *5th IEEE Int'l Conf. on Image Processing*, Chicago, IL, Oct 4-7, (1998).

[3] A. Efros, T. Leung, Texture synthesis by non-parametric sampling, *ICCV* , 2,(1999), 1033-1038.

[4] J. Wu, Q. Ruan, Object removal by cross isophotes exemplar-based inpainting, *Proceedings of the 18th International Conference on Pattern Recognition (ICPR'06)* , Washington, DC, USA,(2006) , 810-813.

[5] N. Komodakis, Image completion using global optimization, *Proceedings of the 2006 IEEE Computer Society Conference on Computer Vision and Pattern Recognition*, Washington, DC, USA,(2006), 442-452.

[6] M. Bertalmio, G. Sapiro, V. Caselles, C. Ballester, Image inpainting, *SIGGRAPH 2000, Computer Graphics Proceedings*, K. Akeley, Ed. ACM Press/ACM SIGGRAPH, Addison Wesley Longman (2000), 417-424.

[7] P. Perona, J. Malik, Scale-space and edge detection using anisotropic diffusion *IEEE Trans. Pattern Anal. Machine Intell.*, 12 (1990), 629-639.

[8] M. Bertalmio, A. Bertozzi, G. Sapiro, Navier-Stokes, fluid dynamics, and image and video inpainting *IEEE Computer Visin and Pattern Recogn. (CVPR), Hawaii*, 1 (2001), I355-I362.

[9] T.F. Chan, J. Shen Mathematical Models of local non-texture inpaintings *SIAM Jou. on Appl. Math.*, 62-3 (2001), 1019-1043.

[10] L. Rudin, S. Osher, E. Fatemi Non linear total variation based noise removal algorithms *Physica D*, 60 (1992), 259-268.

[11] S. Kang, T. Chan, J. Shen, Euler's elastica and curvature-based image inpainting *SIAM Journal on Appl. Math*, 63-2 (2002), 564-592.

[12] S. Esedoglu, J.Shen, Digital inpainting based on the Mumford-Shah image model *European Journal of Appl. Math*, 13 (2002), 353-370.

[13] D.Mumford, J.Shah, Optimal approximations by piece-wise smooth functions and associated variational problems *Communications on Pure and Appl. Math*, 42 (1989), 577-685.

[14] L. Ambrosio, V.M. Tortorelli, Approximations of functionals depending on jumps by elliptic functionals via gamma convergence *Communications on Pure and Appl. Math*, 43 (1990), 999-1030.

[15] D.Eyre An Unconditionally Stable One-Step Scheme for Gradient System, (1998).

[16] A. Bertozzi, S. Esedoglu, A. Gillette Inpainting of binary images using the Cahn-Hilliard equation *IEEE Trans. on Image Processing*, 16-1 (2007), 285-291.

[17] A. Bertozzi, S. Esedoglu, A. Gillette Analysis of a two scale Cahn-Hilliard model for image inpainting *Multiscale moduling and simulation*, vol 6-3 (2007), 913-936.

[18] A.L. Yuille, A. Rangarajan The concave-convex procedure *Neural Computation*, vol 15-4 (2003), 915-936.

[19] L. Dongsun, J.Y. Hu, D. Jeong, J. Shin, A. Yun, J. Kim Physical, mathematical, and numerical derivation of the Cahn-Hilliard equation *Computational Materials Science*, vol 81 (2014), 216-225.